Journal of Materials Chemistry A

ROYAL SOCIETY OF CHEMISTRY

PAPER

View Article Online
View Journal

Cite this: DOI: 10.1039/d6ta03292c

Polymer additives enhance charge transport balance in Y6 single-component organic solar cells

Jiyeon Oh,[a] Xiaowei Zhong,[a] Subhrangsu Mukherjee,[b] Harald Ade,[b] Liang Yan[a] and Wei You*[a]

The discovery of Y6 marks a considerable milestone in the development of bulk heterojunction (BHJ) organic solar cells (OSCs). The unique characteristics of Y6, including a small exciton binding energy and a long exciton diffusion length, have fueled the recent interest in exploring its use as the sole component in OSCs. Others have further shown that the power conversion efficiency (PCE) of such Y6-based single-component OSCs (SC-OSCs) can be enhanced by incorporating a small amount of polymer additives into the photoactive layer, ascribed to improved charge generation and reduced charge recombination. However, these effects have only been observed in specific conjugated polymers in separate studies, and a comprehensive investigation of the impact of different polymer additives and their blending amount on the device characteristics of the Y6-based SC-OSCs has not been performed. In this study, we investigated the influence of four polymer additives on the device performance and charge dynamics of the Y6-based SC-OSC. The additives include two conjugated polymers, poly[(2,6-(4,8-bis(5-(2-ethylhexyl-3-fluoro)thiophen-2-yl)-benzo[1,2-b:4,5-b′]dithiophene))-*alt*-(5,5-(1′,3′-di-2-thienyl-5′,7′-bis(2-ethylhexyl)benzo[1′,2′-c:4′,5′-c′]dithiophene-4,8-dione))] (PM6) and poly(3-hexylthiophene) (P3HT), and two non-conjugated polymers, polyvinylcarbazole (PVK) and polystyrene (PSt). Our results demonstrate that Y6-based SC-OSCs with polymer additives exhibit enhanced hole mobilities and more balanced charge transport, particularly with PM6 and PVK and even in the presence of the insulating polymer PSt, leading to performance enhancements in Y6-based SC-OSCs. Furthermore, the incorporation of PM6 or PVK can effectively reduce bimolecular/trap-assisted recombination, which contributes to improved photovoltaic performance. These results indicate that small amounts of polymer additives can enhance device performance by improving hole transport and suppressing recombination without requiring formation of a conventional donor-rich bulk heterojunction network, providing design guidelines for optimizing charge-transport balance in Y6-based SC-OSCs.

Received 19th April 2026
Accepted 12th May 2026

DOI: 10.1039/d6ta03292c

rsc.li/materials-a

1 Introduction

The advent of non-fullerene acceptors (NFAs) marked a significant turning point in the field of organic solar cells (OSCs).[1–9] The unique properties of NFAs, such as low exciton binding energy, formation of intra-moiety excited states, and extended exciton diffusion lengths, contribute to improved exciton dissociation and enhanced power conversion efficiency (PCE) in bulk heterojunction (BHJ) solar cells.[10–17] Inspired by these remarkable properties of NFAs, researchers have begun to explore NFAs as stand-alone photoactive materials for solar cells (*i.e.*, single-component organic solar cells, SC-OSCs).[18–22] For example, Hodgkiss and co-workers reported that Y6, one of the best performing NFAs, could spontaneously generate free charge carriers.[23] In another study, Mahadevan *et al.* applied electroabsorption spectroscopy to investigate the efficient charge generation by Y6 and their results indicated that a strong charge-transfer (CT) character of the Y6 aggregates could play a key role in the observed charge generation in pure Y6.[24]

However, Y6-based SC-OSCs suffer from low PCEs (typically in the range of 1–2%) owing to severe bimolecular recombination and the presence of hole traps.[25,26] These challenges can be partially mitigated by incorporating a small amount of donor polymers (*e.g.*, PM6).[18,19,21,27] For example, Lin and co-workers demonstrated high-performance SC-OSCs with an impressive PCE of 3.07% using a derivative of Y6 as the photoactive material;[22] however, the PCE could be further enhanced to 3.94% by incorporating as little as 1 wt% of PM6 as the donor polymer into the photoactive layer. This improvement was attributed to an increase in charge-carrier lifetime, leading to an extended electron diffusion length while retaining a reasonably high hole mobility and negligible bimolecular recombination.

[a]*Department of Chemistry, University of North Carolina at Chapel Hill, Chapel Hill, North Carolina, 27599, USA. E-mail: wyou@unc.edu*

[b]*Department of Physics and Organic and Carbon Electronics Laboratories (ORaCEL), North Carolina State University, Raleigh, North Carolina 27695, USA*

While adding a small amount (*e.g.*, 5 wt%) of donor polymers clearly improves the performance of SC-OSCs, almost all prior studies focused on donor polymers that have been successfully used in NFA based BHJ solar cells – such as PM6 and D18 series.[21,28,29] Since these polymers are optically and electronically active, it can be difficult to evaluate the exact function of such donor polymers in SC-OSCs. For example, while 1 wt% donor polymers in Y6 are likely very diluted and not forming an inter-connected polymer network, higher wt% donor polymers (*e.g.*, 10 wt%) could already surpass the percolation threshold and result in a BHJ-like solar cell (rather than the intended SC-OSC) and complicate the data interpretation.[21,29] To delineate the exact function of such polymers in SC-OSCs, one needs to carry out more comprehensive studies that should include different types of polymers at different mixing ratios.

In this study, we address this outstanding question by systematically comparing four polymers blended with Y6-based SC-OSCs over a range of mixing ratios. Through this investigation, we aim to clarify the mechanistic roles of polymer additives and advance the understanding of how they influence device performance in Y6-based SC-OSCs. The selected polymers span a broad range of electronic characteristics and functions, rather than being limited to conventional donor polymers typically used in bulk heterojunction (BHJ) systems, enabling us to distinguish the contributions of electronic character, charge transport, and generic additive effects.

Specifically, we chose two conjugated donor polymers, poly[(2,6-(4,8-bis(5-(2-ethylhexyl-3-fluoro)thiophen-2-yl)-benzo[1,2-b:4,5-b′]dithiophene))-*alt*-(5,5-(1′,3′-di-2-thienyl-5′,7′-bis(2-ethylhexyl)benzo[1′,2′-c:4′,5′-c′]dithiophene-4,8-dione))] (PM6) and poly(3-hexylthiophene) (P3HT), together with two non-conjugated polymers, poly(vinyl carbazole) (PVK) and polystyrene (PSt). The conjugated polymers selected are among the most widely studied donor materials in BHJ OSCs. PM6 is known to achieve high power conversion efficiencies (PCEs) exceeding 15% when paired with Y6, whereas P3HT typically yields lower efficiencies (<3%) due to less favorable energy-level alignment and morphology.[6,30,31] These two materials therefore serve as useful benchmarks representing donor polymers with contrasting performance in Y6-based systems.

As non-conjugated polymer additives, PVK was selected because of its intrinsic hole-transport capability and its widespread use as a hole-transporting material in organic electronic devices.[13,32] Its large band gap forms a type-I heterojunction with Y6, rendering PVK effectively non-photoactive while maintaining favorable HOMO alignment for hole transport. This allows PVK to serve as a functional analogue to conjugated additives for isolating the role of charge transport in determining device performance. In contrast, PSt, an electrically insulating polymer, was chosen as a reference material to isolate morphological or dilution effects of the polymer additive,[33] providing a baseline for determining whether the observed performance changes originate mainly from generic polymer-additive effects rather than electronic contributions.

Our results show that all polymer additives improve the power conversion efficiencies (PCEs) of Y6-based SC-OSCs relative to additive-free devices. Notably, devices containing 5 wt% PM6 and 5 wt% PVK achieved PCEs of 5.39% and 2.32%, respectively, significantly higher than that of the Y6-only device (1.41%). Through a detailed investigation of the optical/morphological properties, charge transport, and charge generation–recombination processes, we found that SC-OSCs processed with appropriate polymer additives (*e.g.*, PM6 and PVK) exhibited higher hole mobilities and more balanced charge carrier mobilities, as well as suppressed bimolecular and trap-assisted recombination when compared to Y6 only devices, collectively accounting for the enhanced PCEs. Moreover, even the electrically insulating additive PSt produces a modest efficiency improvement, which correlates with a slight increase in hole mobility and improved balance in charge transport, suggesting that generic polymer-additive effects can also contribute to performance enhancement.

2 Results and discussion

2.1 Optical properties and microstructure

The chemical structures of the primary component (Y6) and polymer additives (conjugated polymers: PM6 and P3HT; non-conjugated polymers: PVK and PSt) are shown in Fig. 1a. Since the conjugated polymer additives employed in this study are typically used as the donor polymers in BHJ solar cells and significantly participate in the exciton and charge generation processes when blended with NFAs, we needed to determine whether these conjugated polymers act as additives in SC-OSCs or as donor polymers in BHJ OSCs.[34,35]

We first examined the optical properties of Y6-based thin films with varying concentrations of different additives (0, 5, 20, and 100 wt% relative to Y6), as shown in Fig. 1b–e and S1. For films containing conjugated polymer additives, noticeable changes are visible in the absorption spectra starting from 20 wt%, whereas films containing non-conjugated polymer additives show negligible changes even at high blending ratios (*e.g.*, 100 wt%). This observation suggests that the conjugated polymers indeed contribute toward light absorption (and exciton generation) above a certain threshold (20 wt%); below this threshold, they have a minimal impact on the light absorption of the active layer.

In general, the addition of polymer additives in the active layer of BHJ OSCs can have a great influence on the film microstructures and thereby photovoltaic performance.[36–38] To investigate the influence of polymer additives on the microstructures of the corresponding films, we applied the grazing-incidence wide-angle X-ray scattering (GIWAXS) method to evaluate Y6-based films with different additives at various concentrations (0, 5, and 100 wt%) (Fig. S2). The relevant parameters are summarized in Table S1. The pristine Y6 film exhibits a pronounced (010) peak in the out-of-plane direction, suggesting efficient π–π stacking and a preferential face-on orientation. For all films processed with 5 wt% additives, we observed similar locations and *d*-spacing values for the (010) peak, but the crystallite coherence lengths of the (010) peaks decrease slightly, indicating that a small amount of polymer has little effect on π–π stacking but slightly reduces the crystalline domain of Y6. In contrast, for films containing higher additive

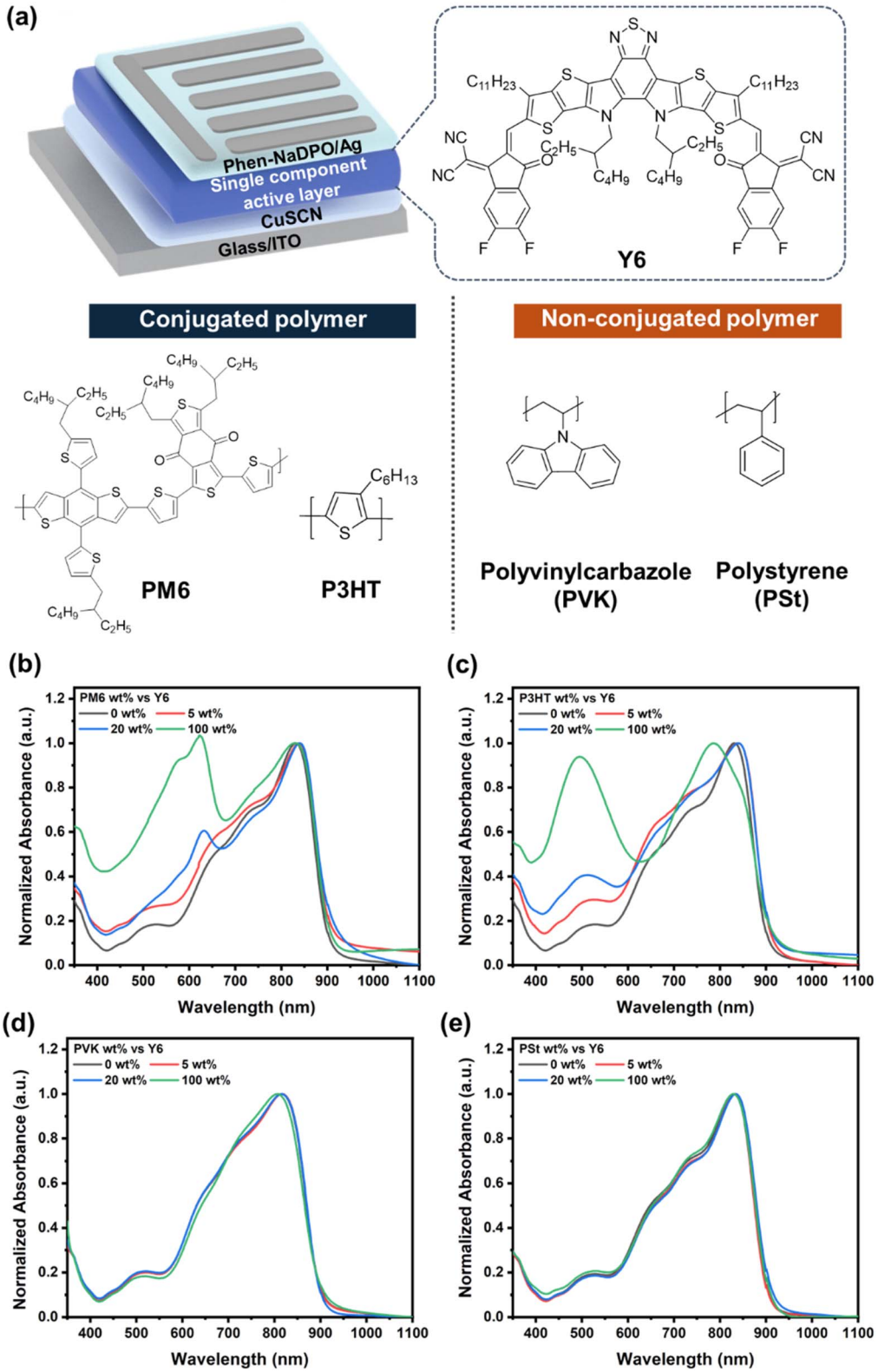

Fig. 1 (a) Device architectures with chemical structures of polymer additives. Normalized UV-vis spectra of SC-OSCs with polymer additives at different concentrations (0, 5, 20, and 100 wt%): (b) PM6, (c) P3HT, (d) PVK, and (e) PSt.

concentrations (100 wt%) (*i.e.*, equivalent to the BHJ system), distinct microstructural changes are clearly visible. These include the appearance of a new peak in the films with non-conjugated polymers additives and changes in both the *d*-spacing and crystallite coherence lengths across all films, indicating that a high content of polymer additives disrupts the

Table 1 Summary of photovoltaic parameters of Y6-based devices with different contents of polymer additive under AM 1.5 G illumination (100 mW cm^{-2})

System	Additive wt% *vs.* Y6	V_{OC}[a] (V)	J_{SC}[a] (mA cm^{-2})	J_{cal} (mA cm^{-2})	FF[a] (%)	PCE[a] (%)
Y6		0.760 (0.745 ± 0.002)	4.02 (3.72 ± 0.28)	3.89	46.13 (45.5 ± 0.34)	1.41 (1.25 ± 0.10)
Y6 : PM6	5	0.758 (0.762 ± 0.005)	13.05 (12.94 ± 0.33)	12.86	54.50 (54.2 ± 0.17)	5.39 (5.04 ± 0.29)
	20	0.760 (0.761 ± 0.004)	20.15 (19.79 ± 0.55)	19.43	67.82 (67.6 ± 0.31)	10.39 (9.83 ± 0.41)
	100	0.769 (0.771 ± 0.008)	20.92 (20.54 ± 0.41)	20.42	67.82 (67.6 ± 0.31)	10.39 (9.83 ± 0.41)
Y6 : P3HT	5	0.552 (0.542 ± 0.003)	6.73 (6.23 ± 0.47)	6.62	41.95 (41.14 ± 0.52)	1.56 (1.24 ± 0.18)
	20	0.560 (0.559 ± 0.005)	11.61 (11.57 ± 0.33)	11.17	38.86 (38.61 ± 0.39)	2.53 (2.50 ± 0.19)
	100	0.552 (0.549 ± 0.009)	2.70 (2.43 ± 0.27)	2.79	31.24 (31.21 ± 0.39)	0.47 (0.42 ± 0.04)
Y6 : PVK	5	0.759 (0.758 ± 0.01)	6.43 (6.14 ± 0.32)	6.22	47.59 (47.25 ± 0.53)	2.32 (2.19 ± 0.11)
	20	0.758 (0.758 ± 0.001)	4.64 (4.45 ± 0.26)	4.47	41.83 (41.74 ± 0.58)	1.48 (1.41 ± 0.08)
	100	0.757 (0.758 ± 0.008)	2.58 (2.18 ± 0.31)	2.52	45.23 (44.66 ± 0.27)	0.88 (0.74 ± 0.10)
Y6 : PSt	5	0.755 (0.744 ± 0.01)	5.08 (4.85 ± 0.38)	4.94	45.46 (45.18 ± 0.45)	1.72 (1.59 ± 0.14)
	20	0.761 (0.760 ± 0.003)	2.89 (2.78 ± 0.20)	2.72	43.71 (43.13 ± 0.40)	0.96 (0.83 ± 0.26)
	100	0.690 (0.684 ± 0.006)	0.94 (0.93 ± 0.02)	0.95	37.11 (36.69 ± 0.45)	0.24 (0.23 ± 0.04)

[a] The average values with standard deviations in parentheses are obtained from 12 cells.

crystalline structure of Y6 or forms their own domains. Collectively, these results suggest that small amounts of additives appear to mix well with Y6 and do not disrupt the π–π ordering of the Y6 matrix.

2.2 Photovoltaic performance

We next evaluated how the polymer additives would affect the device performance of Y6-based SC-OSCs. We fabricated SC-OSCs with the following structure: indium tin oxide (ITO)/CuSCN/Y6/3-(6-diphenylphosphorylnaphthalen-2-yl)-1,10-phenanthroline (Phen-NaDPO)/Ag (Fig. 1a). We first optimized the Y6-only SC-OSCs as a control device by adjusting the cosolvent composition (a mixture of chloroform (CF) and chlorobenzene (CB)). The active layer was spin-coated and subsequently thermally annealed at 100 °C for 10 min (refer to the Experimental Section for detailed device fabrication procedures). The optimized conditions are presented in Table 1 and S2 of the SI. The control Y6 device without additives exhibits an optimal PCE of 1.41%, including a short-circuit current density (J_{SC}) of 4.02 mA cm^{-2}, an open-circuit voltage (V_{OC}) of 0.760 V, and a fill factor (FF) of 46.1%. We then evaluated the effects of additive loading (1, 5, 10, 20, 50, and 100 wt% relative to Y6) on the device performance of Y6-based SC-OSCs fabricated under identical conditions (*vide supra*). The representative current density–voltage (*J–V*) characteristics of all devices measured under simulated AM 1.5 G conditions (100 mW cm^{-2}) are shown in Fig. S3, and the corresponding parameters are summarized in Table 1 and S3–S6.

Compared to the control device (Y6 only), we observed an improvement in PCE with all additives—though appearing at different wt%, depending upon the chemical nature of the polymer additive. Specifically, devices incorporating PM6 exhibit a sharp increase in PCE with the increasing additive content up to 20 wt% (Fig. 2a), beyond which the performance saturates. This saturation trend is indicative of a transition to a BHJ regime. In contrast, although P3HT is also a conjugated polymer, it exhibits a different trend in the observed efficiency (Fig. 2b). The PCE remains nearly unchanged up to 10 wt% and then shows a noticeable increase at 20 wt% with the highest efficiency at 2.53%; thereafter the PCE declines with higher wt% of P3HT. This behavior suggests that P3HT does not function effectively in the BHJ system when blended with Y6, as previously reported.[39] This peculiar behavior has been ascribed to the high miscibility between PH3T and Y6, which suppresses phase separation and the formation of an optimal donor–acceptor morphology required for efficient charge generation and transport.[39]

On the other hand, both non-conjugated polymer additives (PVK and PSt) demonstrate a similar trend to that of P3HT, although the peak efficiency appears at lower wt% values (Fig. 2c and d). Both additives yield their highest PCEs at 5 wt%—2.38% for PVK and 1.72% for PSt, beyond which the performance gradually declines at higher concentrations. This observation is likely due to their intrinsically insulating nature that can hinder charge transport when present in large excess.[40,41] Unlike conjugated polymers, PVK and PSt do not contribute to exciton generation due to their lack of absorption in the visible region. Nevertheless, the observed performance enhancement at low concentrations suggests that small amounts of non-conjugated additives can also improve the PCEs of Y6-based SC-OSCs. To highlight the loading-dependent trends discussed above, particularly the distinct behaviors at 5 wt% and 20 wt%, we added a summary graph (Fig. S4) comparing the device metrics at these two additive contents across all polymer additives.

To gain a better understanding of the origin of this performance enhancement, we analyzed the external quantum efficiency (EQE) spectra of the corresponding devices. As depicted in Fig. S5, EQE spectra of all Y6-based SC-OSCs with additives exhibit photovoltaic responses in the wavelength range of 350–900 nm, mirroring the trend observed in the J_{SC} values from the *J–V* curves (Tables S3–S6). Notably, an enhancement in EQE across the entire wavelength range is clearly visible in devices containing the optimal additive concentration, indicating that the EQE increase is not accompanied by a distinct new spectral feature from the polymer additives. The EQE also shows a strong loading

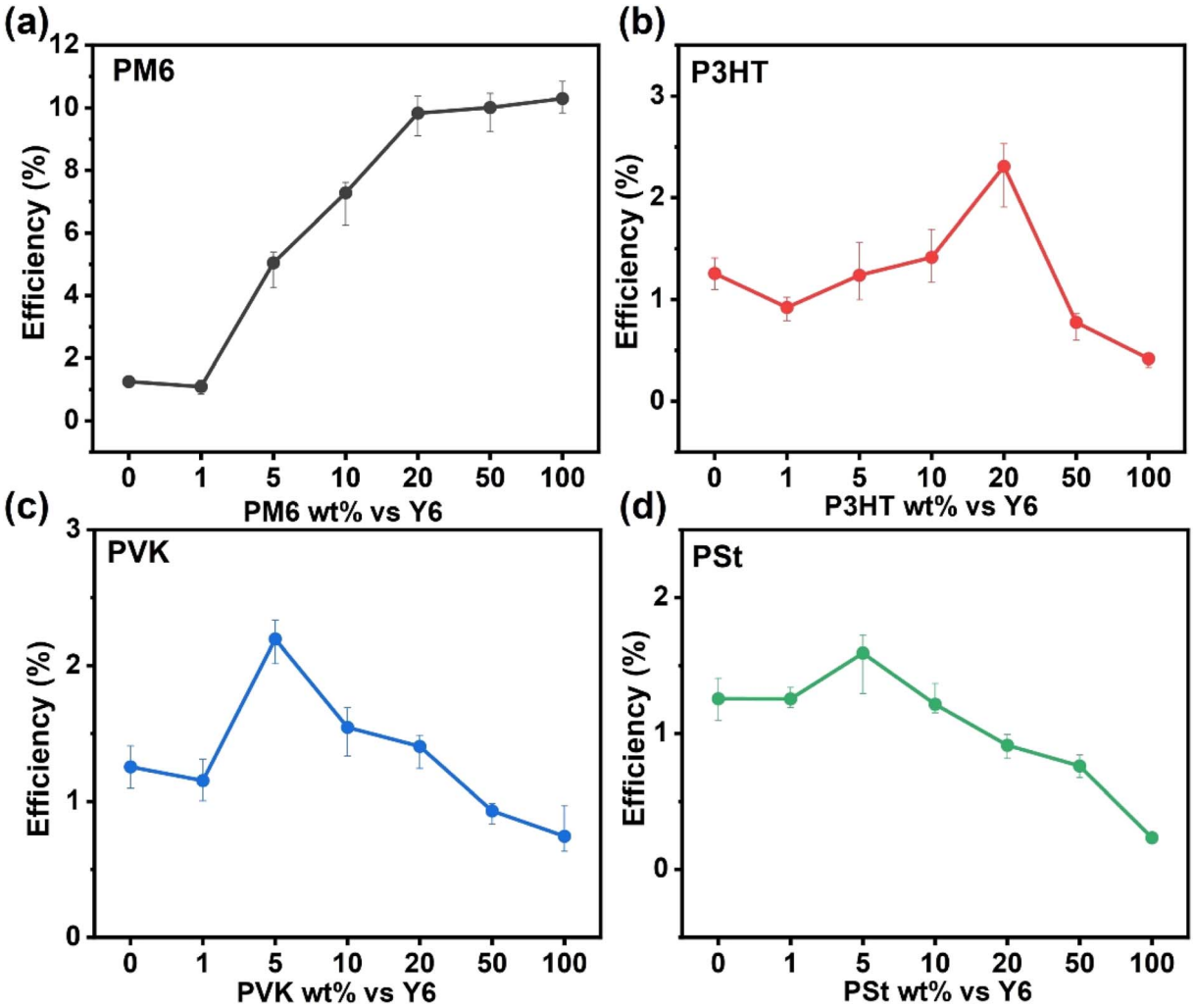

Fig. 2 PCE trend of Y6-based devices depending on the content of (a) PM6-, (b) P3HT-, (c) PVK-, and (d) PSt-polymer additive (1, 5, 10, 20, 50, and 100 wt%).

dependence, and the trend differs by polymer type. For PM6, the EQE increases markedly with loading and then reaches a plateau beyond ~20 wt%, showing only minor differences between 20, 50, and 100 wt%. In contrast, P3HT shows a maximum EQE at ~20 wt% followed by a decrease at higher loadings, while the non-conjugated additives (PVK and PSt) exhibit their highest EQE at low loadings (typically 5–10 wt%) and gradually decrease when the additive contents increase. These distinct loading-dependent behaviors indicate that the device photoresponse is not governed solely by changes in optical absorption, which can vary with thickness and composition, but is strongly influenced by how effectively photogenerated carriers are extracted under each additive-loading condition. This observation suggests that, rather than enhanced exciton generation through additional light absorption by the polymer additives (*e.g.*, non-conjugated polymers do not even absorb in this spectral region), other factors must contribute to the improved performance of the SC-OSCs: for example, charge-carrier dynamics.[29] These aspects were subsequently analyzed and will be discussed in the following section.

2.3 Charge-carrier dissociation, transport, and recombination dynamics

To further understand the working principles underlying the impact of polymer additives on the performance of Y6-based SC-OSCs, we next performed a detailed analysis on charge dynamics, including exciton dissociation, charge generation, charge transport, and recombination. We focused on samples containing 5, 20, and 100 wt% polymer additives as these concentrations capture the key difference in the device performance for each additive. Specifically, 20 wt% gave the highest performance in the case of conjugated polymers (PM6 and P3HT), while 5 wt% resulted in the best performance for non-conjugated polymers (PVK and PSt). In addition, 100 wt% was included as a reference representing a typical BHJ system, to compare with additive-based systems at lower concentrations.

2.3.1 Photoluminescence quenching and charge-carrier dissociation. First, we employed photoluminescence (PL) quenching efficiency measurements to investigate the exciton dissociation properties. As illustrated in Fig. S6, the pristine Y6 film exhibits distinct PL spectra with maximum emission peaks

at 920 and 1080 nm, respectively. As expected, Y6 films with conjugated polymers (PM6 or P3HT) exhibit efficient PL quenching; for P3HT, 98% quenching efficiency was noted even at 5 wt%. In contrast, PM6-based systems show a gradual increase in PL quenching efficiency with an increasing amount of additive, reaching comparable quenching levels (to that of P3HT at 5 wt%) only at 20 wt%. Despite the difference in the quenching behavior, the trend in device performance is reversed. PM6-based devices show a steady increase in PCE, which correlates with the increase in the PL quenching efficiency, while P3HT-based devices exhibit low PCEs at low concentrations where exciton quenching is already efficient. These results suggest that efficient exciton dissociation alone is not sufficient to ensure high device performance; thus, additional factors beyond exciton dissociation would contribute considerably to the observed trend in PCE.

In the case of non-conjugated polymer additives (PVK and PSt), the PL quenching is generally negligible, except for the 5 and 20 wt% PVK samples, where moderate quenching is notable (Fig. S6c and d). This quenching behavior may be attributed to trap-induced effects or local variations in the morphological or electronic environment, potentially arising from energetic disorder or polar interactions at the interface. Furthermore, the observed PL quenching may also be ascribed to trap-assisted nonradiative recombination, which is commonly observed in the energetically disordered or aggregated domains.[42] These results suggest that while non-conjugated additives generally do not promote exciton dissociation, specific polymers such as PVK may still affect exciton behavior through subtle morphological or trap-related effects. Collectively, these findings highlight that the different behavior in PL quenching is not strongly correlated with the difference in the device performance of Y6-based SC-OSCs containing these polymer additives, and that both the nature and concentration of the additive should be considered to evaluate its impact on the exciton dissociation and charge generation.

2.3.2 Charge transport. To further elucidate the relationship between additive characteristics and device efficiency, we examined the charge transport and recombination behavior of these systems. Charge-carrier mobilities, including hole mobility (μ_h) and electron mobility (μ_e), were determined using the space-charge-limited current (SCLC) method. Fig. S7 and S8 present the current density–voltage characteristics used for mobility extraction, and the corresponding values are summarized in Table 2. The introduction of polymer additives enhances hole mobility in nearly all cases, except for the device containing 100 wt% PSt, consistent with its strongly insulating nature. Notably, devices incorporating 20 wt% conjugated polymers (PM6 and P3HT) or 5 wt% PVK show clear enhancements in hole mobility relative to the pristine Y6 device. This behavior can be attributed to the intrinsic p-type character of these additives, which facilitates hole transport within the blend. Importantly, the mobility enhancement observed at low additive loading (*e.g.*, 5 wt%) occurs at concentrations likely below the percolation threshold typically associated with formation of a continuous donor-rich bulk heterojunction (BHJ) network. Instead, these results suggest that small amounts of polymer can modulate the local transport landscape within the Y6-rich matrix. At such sub-percolation concentrations, polymer segments may influence the local electronic environment, for example through changes in site-energy disorder, dielectric screening, or trap-mediated hopping pathways. These effects can improve the effective connectivity of hole-transport pathways without requiring substantial morphological reconstruction, leading to enhanced hole mobility and more balanced charge transport (μ_h/μ_e). Consistent with this interpretation, the most pronounced device-level improvements are observed in the fill factor (FF) and short-circuit current density (J_{SC}).

To better understand the origin of the mobility enhancement, we examined film morphology using AFM (Fig. S9). At low additive concentrations, films containing PM6, P3HT, and PVK exhibit surface morphologies broadly comparable to that of pristine Y6, with no significant change in roughness, whereas the film containing 5 wt% PSt appears slightly rougher. Together with GIWAXS results showing minimal structural variation in this composition range, these observations indicate that the enhanced hole mobility at low additive loading is more likely associated with local tuning of the transport environment within the Y6-rich matrix, rather than large-scale morphological reconstruction or bulk structural reorganization. At higher

Table 2 Hole and electron mobilities of the Y6-based device with different contents of polymer additives

System	Additive wt% *vs.* Y6	Hole mobility (10^{-4} cm^2 V^{-1} s^{-1})	Electron mobility (10^{-4} cm^2 V^{-1} s^{-1})	μ_h/μ_e
Y6		1.24 ± 0.09	6.44 ± 0.12	0.19
Y6 : PM6	5	6.04 ± 0.12	10.88 ± 0.14	0.56
	20	6.66 ± 0.38	8.50 ± 0.16	0.78
	100	7.78 ± 0.30	6.12 ± 0.18	1.27
Y6 : P3HT	5	2.62 ± 0.21	7.25 ± 0.26	0.36
	20	4.10 ± 0.41	5.45 ± 0.26	0.75
	100	3.51 ± 0.33	0.13 ± 0.02	27
Y6 : PVK	5	5.31 ± 0.14	6.75 ± 0.22	0.79
	20	5.55 ± 0.29	6.52 ± 0.10	0.85
	100	2.72 ± 0.30	2.03 ± 0.12	1.34
Y6 : PSt	5	2.25 ± 0.16	5.15 ± 0.13	0.44
	20	2.02 ± 0.24	3.96 ± 0.24	0.51
	100	0.15 ± 0.02	0.80 ± 0.13	0.19

additive loadings, the morphology becomes increasingly polymer-dependent, with more pronounced roughening observed for PVK and especially PSt, while PM6 exhibits a morphology relatively similar to pristine Y6 over a broader composition range.

In contrast, electron mobilities in devices containing moderate amounts of polymer additives (*e.g.*, 20 wt% conjugated polymers or 5 wt% PVK) either increase slightly or remain comparable to those of Y6-only devices, but decrease at higher additive concentrations. Notably, devices incorporating 20 wt% conjugated polymers or 5 wt% PVK exhibit substantially more balanced charge transport, with μ_h/μ_e ratios approaching unity (for example, 0.78 for 20 wt% PM6) compared with the control Y6-only device (0.19) (Table 2). These results indicate that an optimal amount of polymer additive can improve hole transport and charge collection, contributing to the higher J_{SC} values observed in this study (Table 1), while also promoting more balanced ambipolar transport in Y6-based SC-OSCs.

Although enhanced hole mobility contributes to improved device performance, it does not solely determine the overall efficiency. Rather, device performance is governed by the interplay of charge-transport balance, recombination dynamics, and charge collection, as discussed below. Additionally, although more balanced mobilities generally improve the FF,[21,43,44] our results suggest that J_{SC} plays a more important role in deciding the trend in the PCE.

2.3.3 Charge collection and recombination dynamics. Considering that both J_{SC} and V_{OC} are also strongly influenced by recombination dynamics, we next analyzed the effect of polymer additives on carrier recombination behavior by examining the light-intensity dependence of the *J–V* characteristics. The relationship between J_{SC} and P_{light} is typically described by a power-law equation [$J_{SC} \propto (P_{light})^{\alpha}$], where α is the exponential factor and its value indicates the extent of bimolecular recombination.[45] Compared with the Y6-only device ($\alpha = 0.819$), we obtained higher α values for all PM6-containing devices (0.949–0.984), indicating effective suppression of bimolecular recombination. In contrast, P3HT-containing devices exhibit significantly lower α values (0.658–0.768), consistent with their inferior device performance (Fig. 3a). As for non-conjugated polymer systems, only the device containing 5 wt% PVK shows a slightly improved α value (0.835), whereas all PSt-based devices exhibit decreased values, indicating more pronounced recombination. Notably, the trend in the α value closely matches the trend of J_{SC} values observed in the corresponding devices, further suggesting that the recombination loss is a key factor limiting photocurrent generation in less efficient systems. On the other hand, the V_{OC} as a function of light intensity is described by the equation $V_{OC} \propto \ln(P_{light})nkT/q$, where k is the Boltzmann constant, T is the temperature in Kelvin, and q is the elementary charge.[46] Here the slope (n) can be used to assess the trap-assisted recombination. As shown in Fig. 3b, PM6-based devices exhibit lower slopes (1.118–1.263) compared to the Y6-only device (1.680), indicating reduced trap-assisted recombination. Likewise, the 5 wt% PVK-based device also shows a lower slope (1.492), whereas other systems do not show notable improvement. These results suggest suppressed bimolecular recombination and reduced trap-assisted recombination loss in devices containing PM6 and 5 wt% PVK. It should be noted that a reduced slope reflects a smaller contribution from trap-assisted recombination, but does not necessarily translate into increased V_{OC}. In our device architecture, V_{OC} is also strongly constrained by the energetics of the interfacial selective layers, consistent with the nearly unchanged V_{OC} values observed for the PM6- and PVK-containing devices despite their reduced slopes.[28]

To further evaluate when the system begins to exhibit BHJ-like behavior, we define the onset operationally based on the loading-dependent recombination signatures (Fig. S10). Within this framework, a shift toward higher α (approaching unity), lower kT/q slopes, and saturation of J_{SC} and PCE with increasing additive loading is taken as evidence of BHJ-like operation. Using these criteria, PM6 is the only additive that shows a clear transition toward BHJ-like behavior, with the transition emerging at low loading and becoming well established around 20 wt%. In contrast, P3HT does not exhibit a stable BHJ-like evolution, while PVK and PSt are more consistently interpreted in terms of local transport modulation or dilution effects, rather than formation of a donor-type heterojunction.

To further elucidate the characteristics of charge dynamics, we measured the dependence of photocurrent (J_{ph}) on the effective voltage (V_{eff}), as shown in Fig. S11. The photocurrent is defined as $J_{ph} = J_L - J_D$, where J_L and J_D represent the current densities measured under illumination and in the dark, respectively. The effective voltage is given by $V_{eff} = V_0 - V$, where V_0 is the compensation voltage when $J_{ph} = 0$, and V is the applied voltage. The exciton dissociation probabilities ($P_{diss} = J_{ph}^{SC}/J_{sat}$) and charge collection efficiencies ($P_{coll} = J_{ph}^{max}/J_{sat}$) for devices containing the optimal additive loadings were calculated and are summarized in Fig. 4 and Table S7. As shown in Fig. 4, PM6-based devices exhibit significantly higher exciton dissociation probabilities and charge collection efficiencies than the Y6-only device. In contrast, P3HT-containing devices show lower values in both metrics, indicating that not all conjugated polymer additives (*e.g.*, PM6 *vs.* P3HT) contribute equally to charge extraction. Among the non-conjugated systems, the device containing 5 wt% PVK shows a noticeable improvement, with the exciton dissociation probability and charge collection efficiency approaching ~70% and ~60%, respectively, whereas devices with PSt show only minor increases or even decreases. These trends are consistent with the SCLC and light-intensity-dependent *J–V* analyses, further supporting that charge dynamics play a key role in determining device performance. Notably, the *J–V* plots indicate that J_{ph} nearly saturates for $V_{eff} > 1$ V only in PM6-containing devices, while for other additive-containingdevices J_{ph} does not saturate even at $V_{eff} = 3$ V and continues to increase with higher bias, suggesting that the PM6 additive effectively suppresses geminate and bimolecular recombination.[47,48] It is worth noting that the values obtained for other devices may still be overestimated; nevertheless, they adequately capture the overall trend.

Taken together, these results suggest that the improved photovoltaic performance of PM6-based devices (5, 20, and 100 wt%) and PVK-based devices (5 wt%) originates from more

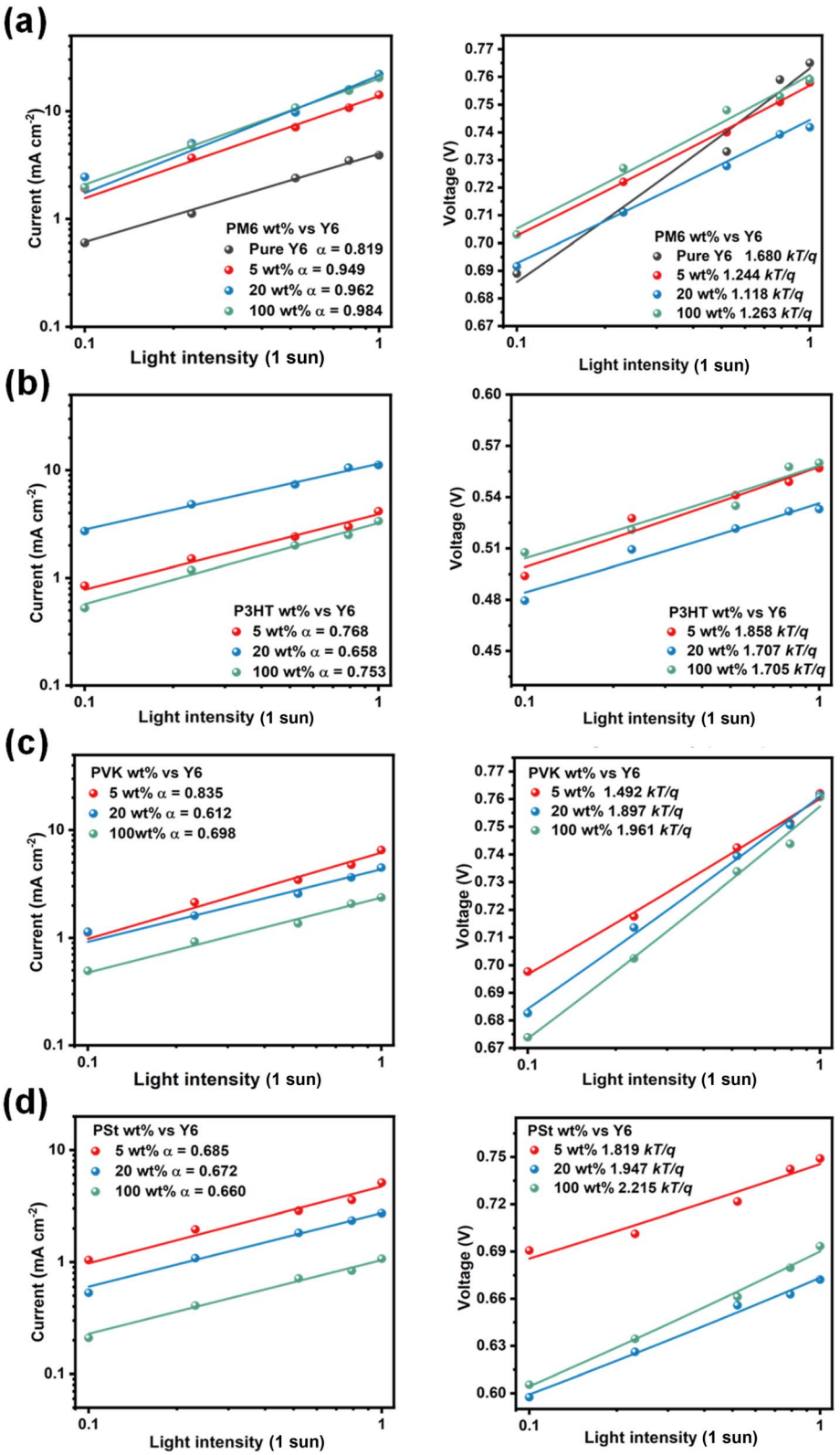

Fig. 3 Light-intensity-dependent short-circuit current density (left panels) and open-circuit voltage (right panels) of SC-OSCs with (a) PM6, (b) P3HT, (c) PVK, and (d) PSt polymer additives at 5, 20, and 100 wt%.

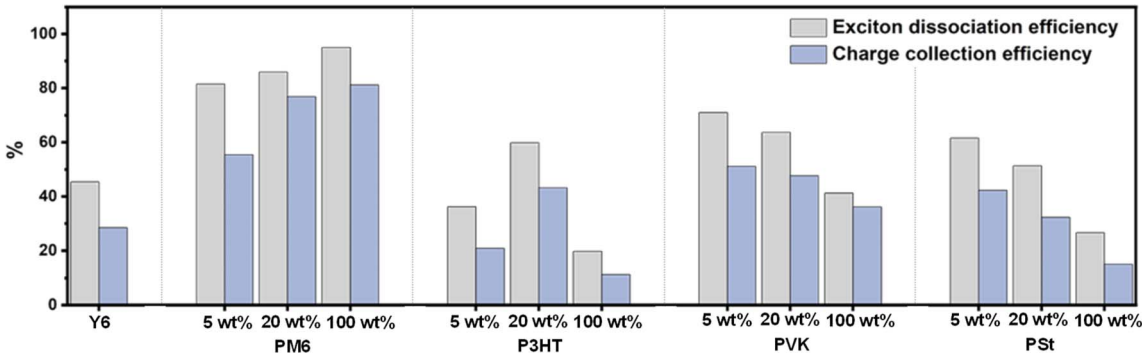

Fig. 4 Exciton dissociation probability and charge collection efficiency under short-circuit and maximum power output conditions.

efficient charge generation, extraction, and suppressed recombination losses. These findings underscore the importance of tuning both the type and concentration of polymer additives to optimize charge dynamics in SC-OSC systems for higher PCEs.

2.4 Overall impacts of polymer additives in Y6-based SC-OSCs

While small amounts of polymer additives do not significantly alter the optical absorption or π–π stacking of Y6 films, pronounced differences in charge dynamics and device performance emerge depending on the identity and concentration of the additive. For conjugated polymer additives, both PM6 and P3HT facilitate exciton dissociation; however, only PM6 leads to substantial improvements in charge transport and suppression of recombination losses. The combined enhancement in charge mobility, transport balance, and recombination dynamics results in the highest observed PCE (5.39%) for devices containing 20 wt% PM6.

In contrast, although P3HT-containing devices exhibit efficient photoluminescence quenching, the overall performance improvement remains limited, indicating that efficient exciton dissociation alone is insufficient to achieve high device efficiency. Instead, charge mobility and recombination characteristics play a more decisive role in determining device performance.

For non-conjugated polymer additives, the improvements are more moderate. PVK at 5 wt% enhances key device parameters, which can be attributed to its favorable influence on hole mobility and recombination dynamics, as supported by light-intensity-dependent and charge-extraction analyses. In comparison, PSt, a purely insulating polymer, shows minimal or even negative impact on device performance, consistent with its limited electronic interaction with the photoactive Y6 matrix. The observation that PVK and PSt still provide measurable performance improvements suggests that conjugation is not strictly required for enhaning SC-OSC performance. Instead, modification of the local dielectric environment, free-volume distribution, or energetic disorder may contribute to improved charge transport and collection in the Y6-rich matrix.

Taken together, these results demonstrate that appropriately selected polymer additives can strongly influence charge generation, transport, and recombination in Y6-based SC-OSCs. In particular, PM6 (20 wt%) and PVK (5 wt%) provide the most balanced and synergistic improvements, highlighting the importance of rational additive selection and concentration optimization for achieving high-performance single-component devices.

3 Conclusion

In summary, we investigated four polymer additives (PM6, P3HT, PVK, and PSt) and their effects on photovoltaic performance of Y6-based SC-OSCs. At low loading (5 wt%), the additives do not significantly alter the absorption spectra or microstructure of the Y6 films, indicating that even conjugated polymers such as PM6 and P3HT contribute minimally to exciton generation in this regime. This behavior differs fundamentally from conventional BHJ devices, in which the donor polymer typically constitutes ~50 wt% of the photoactive layer and plays a major role in light absorption and exciton generation.

While all additives at 5 wt% improve device performance, PM6 and PVK are particularly effective at this low concentration, increasing the PCE of Y6-based SC-OSCs from 1.41% to 5.39% and 2.32%, respectively. Devices incorporating polymer additives generally exhibit higher hole mobility and more balanced charge-carrier transport, with the effect being most pronounced for PM6 and PVK. In these cases, the conjugated or hole-transporting additives facilitate more efficient hole transport within the Y6 matrix, consistent with their intrinsic p-type character.

Interestingly, a similar trend is also observed in devices processed with the insulating polymer PSt, where a moderate increase in hole mobility at low loading is accompanied by slightly enhanced crystallinity of the Y6 domains (reduced *d*-spacing and increased coherence length). This observation suggests that polymer additives can improve the performance of Y6-based SC-OSCs that are limited by low hole mobility and unbalanced charge transport, even in the absence of strong electronic interactions.

In addition, devices incorporating PM6 or PVK exhibit suppressed bimolecular and trap-assisted recombination, as evidenced by light-intensity-dependent and effective-voltage analyses, further contributing to the improved photovoltaic

performance. Overall, these results provide useful guidance for improving SC-OSC efficiency through rational selection and optimization of polymer additives.

Conflicts of interest

There are no conflicts to declare.

Data availability

The data supporting this article have been included as part of the supplementary information (SI). Supplementary information: experimental section; GIWAX images; photovoltaic parameters with *J–V* and EQE curves; PL data; SCLC plots; AFM; J_{ph} *versus* V_{eff} plots. See DOI: https://doi.org/10.1039/d6ta03292c.

Acknowledgements

This work was financially supported by the Office of Naval Research (ONR) under Awards N00014-24-1-2107 (to J. O. and W. Y.), N00014-20-1-2181 (to X. Z. and W. Y.), and N00014-23-1-2001 (to L. Y. and W. Y.), and by the National Science Foundation (NSF) under Award CBET-1934351 (to S. M and H. A.). Photoluminescence measurements of this work were performed in the CHASE Hub Instrumentation Facility established by the Center for Hybrid Approaches in Solar Energy to Liquid Fuels (CHASE) at the University of North Carolina at Chapel Hill, an Energy Innovation Hub funded by the U.S. Department of Energy, Office of Science, Office of Basic Energy Sciences under Award Number DE-SC0021173.

References

1 H. Bin, Z.-G. Zhang, L. Gao, S. Chen, L. Zhong, L. Xue, C. Yang and Y. Li, *J. Am. Chem. Soc.*, 2016, **138**, 4657–4664.
2 J. Hou, O. Inganäs, R. H. Friend and F. Gao, *Nat. Mater.*, 2018, **17**, 119–128.
3 Y. Jiang, S. Sun, R. Xu, F. Liu, X. Miao, G. Ran, K. Liu, Y. Yi, W. Zhang and X. Zhu, *Nat. Energy*, 2024, **9**, 975–986.
4 K. Liu, Y. Jiang, G. Ran, F. Liu, W. Zhang and X. Zhu, *Joule*, 2024, **8**, 835–851.
5 C. Yan, S. Barlow, Z. Wang, H. Yan, A. K. Y. Jen, S. R. Marder and X. Zhan, *Nat. Rev. Mater.*, 2018, **3**, 18003.
6 J. Yuan, Y. Zhang, L. Zhou, G. Zhang, H.-L. Yip, T.-K. Lau, X. Lu, C. Zhu, H. Peng, P. A. Johnson, M. Leclerc, Y. Cao, J. Ulanski, Y. Li and Y. Zou, *Joule*, 2019, **3**, 1140–1151.
7 Y. Zhang, K. Liu, J. Huang, X. Xia, J. Cao, G. Zhao, P. W. K. Fong, Y. Zhu, F. Yan, Y. Yang, X. Lu and G. Li, *Nat. Commun.*, 2021, **12**, 4815.
8 F. Zhao, C. Wang and X. Zhan, *Adv. Energy Mater.*, 2018, **8**, 1703147.
9 W. Zhao, S. Li, H. Yao, S. Zhang, Y. Zhang, B. Yang and J. Hou, *J. Am. Chem. Soc.*, 2017, **139**, 7148–7151.
10 Y. Firdaus, V. M. Le Corre, S. Karuthedath, W. Liu, A. Markina, W. Huang, S. Chattopadhyay, M. M. Nahid, M. I. Nugraha, Y. Lin, A. Seitkhan, A. Basu, W. Zhang, I. McCulloch, H. Ade, J. Labram, F. Laquai, D. Andrienko, L. J. A. Koster and T. D. Anthopoulos, *Nat. Commun.*, 2020, **11**, 5220.
11 P. A. Hume, W. Jiao and J. M. Hodgkiss, *J. Mater. Chem. C*, 2021, **9**, 1419–1428.
12 H. Lai, Z. Deng and F. He, *Joule*, 2024, **8**, 572–575.
13 S. Mahadevan, T. Liu, S. M. Pratik, Y. Li, H. Y. Ho, S. Ouyang, X. Lu, H.-L. Yip, P. C. Y. Chow, J.-L. Brédas, V. Coropceanu, S. K. So and S.-W. Tsang, *Nat. Commun.*, 2024, **15**, 2393.
14 K. Wang, S. Jinnai, T. Urakami, H. Sato, M. Higashi, S. Tsujimura, Y. Kobori, R. Adachi, A. Yamakata and Y. Ie, *Angew. Chem., Int. Ed.*, 2024, **63**, e202412691.
15 R. Wang, C. Zhang, Q. Li, Z. Zhang, X. Wang and M. Xiao, *J. Am. Chem. Soc.*, 2020, **142**, 12751–12759.
16 G. Zhang, X.-K. Chen, J. Xiao, P. C. Y. Chow, M. Ren, G. Kupgan, X. Jiao, C. C. S. Chan, X. Du, R. Xia, Z. Chen, J. Yuan, Y. Zhang, S. Zhang, Y. Liu, Y. Zou, H. Yan, K. S. Wong, V. Coropceanu, N. Li, C. J. Brabec, J.-L. Bredas, H.-L. Yip and Y. Cao, *Nat. Commun.*, 2020, **11**, 3943.
17 L. Zhu, J. Zhang, Y. Guo, C. Yang, Y. Yi and Z. Wei, *Angew. Chem., Int. Ed.*, 2021, **60**, 15348–15353.
18 Z. Chen, W. Ma and H. Yan, *J. Mater. Chem. A*, 2023, **11**, 6901–6908.
19 A. Dolan, X. Pan, M. J. Griffith, A. Sharma, J. M. de la Perrelle, D. Baran, G. F. Metha, D. M. Huang, T. W. Kee and M. R. Andersson, *Adv. Mater.*, 2024, **36**, 2309672.
20 E. Sağlamkaya, A. Musiienko, M. S. Shadabroo, B. Sun, S. Chandrabose, O. Shargaieva, G. Lo Gerfo M, N. F. van Hulst and S. Shoaee, *Mater. Horiz.*, 2023, **10**, 1825–1834.
21 N. Yao, J. Wang, Z. Chen, Q. Bian, Y. Xia, R. Zhang, J. Zhang, L. Qin, H. Zhu, Y. Zhang and F. Zhang, *J. Phys. Chem. Lett.*, 2021, **12**, 5039–5044.
22 Z. Zhang, L. Li, C. Xu, P. Jin, M. Huang, Y. Li, H. Wang, Y. Yi, C. Zhang, Y. Yang, W. Xu and Y. Lin, *Cell Rep. Phys. Sci.*, 2022, **3**, 100895.
23 M. B. Price, P. A. Hume, A. Ilina, I. Wagner, R. R. Tamming, K. E. Thorn, W. Jiao, A. Goldingay, P. J. Conaghan, G. Lakhwani, N. J. L. K. Davis, Y. Wang, P. Xue, H. Lu, K. Chen, X. Zhan and J. M. Hodgkiss, *Nat. Commun.*, 2022, **13**, 2827.
24 S. Mahadevan, T. Liu, S. M. Pratik, Y. Li, H. Y. Ho, S. Ouyang, X. Lu, H.-L. Yip, P. C. Y. Chow, J.-L. Brédas, V. Coropceanu, S. K. So and S.-W. Tsang, *Nat. Commun.*, 2024, **15**, 2393.
25 P. A. Hume, M. B. Price and J. M. Hodgkiss, *JACS Au*, 2024, **4**, 1295–1302.
26 Y. Yan, S. Zhao, Y. Zhang, T. Wang, Y. Shi, D. Qiu, J. Zhang, L. Zhu, M. Wang, J. Qiao, X. Hao, X. Zhang and Z. Wei, *Sol. RRL*, 2023, **7**, 2300342.
27 Y. Tang, H. Zheng, X. Zhou, Z. Tang, W. Ma and H. Yan, *Energy Environ. Sci.*, 2023, **16**, 653–662.
28 A. Sharma, J. Gorenflot, H. Xu, J. P. Jurado, S. Alam, D. Rosas Villalva, X. Pan, J. Bertrandie, P. D. Nayak, Y. He, M. Alqurashi, Y. Luo, M. R. Andersson, O. J. Sandberg, F. Laquai and D. Baran, *Energy Environ. Sci.*, 2025, **18**, 7610–7623.
29 Y. Wang, M. B. Price, R. S. Bobba, H. Lu, J. Xue, Y. Wang, M. Li, A. Ilina, P. A. Hume, B. Jia, T. Li, Y. Zhang,

N. J. L. K. Davis, Z. Tang, W. Ma, Q. Qiao, J. M. Hodgkiss and X. Zhan, *Adv. Mater.*, 2022, **34**, 2206717.
30 M. Gao, Y. Liu, K. Xian, Z. Peng, K. Zhou, J. Liu, S. Li, F. Xie, W. Zhao, J. Zhang, X. Jiao and L. Ye, *Aggregate*, 2022, **3**, e190.
31 Q. Guo, Q. Guo, Y. Geng, A. Tang, M. Zhang, M. Du, X. Sun and E. Zhou, *Mater. Chem. Front.*, 2021, **5**, 3257–3280.
32 Q. Chen, H. Huang, D. Hu, C. e. Zhang, X. Xu, H. Lu, Y. Wu, C. Yang and Z. Bo, *Adv. Mater.*, 2023, **35**, 2211372.
33 Y. Huang, W. Wen, S. Mukherjee, H. Ade, E. J. Kramer and G. C. Bazan, *Adv. Mater.*, 2014, **26**, 4168–4172.
34 S. Holliday, R. S. Ashraf, A. Wadsworth, D. Baran, S. A. Yousaf, C. B. Nielsen, C.-H. Tan, S. D. Dimitrov, Z. Shang, N. Gasparini, M. Alamoudi, F. Laquai, C. J. Brabec, A. Salleo, J. R. Durrant and I. McCulloch, *Nat. Commun.*, 2016, **7**, 11585.
35 S. Shoaee, H. M. Luong, J. Song, Y. Zou, T.-Q. Nguyen and D. Neher, *Adv. Mater.*, 2024, **36**, 2302005.
36 T. Kumari, M. Moon, S.-H. Kang and C. Yang, *Nano Energy*, 2016, **24**, 56–62.
37 J. Oh, S. Jung, M. Jeong, B. Lee, J. Lee, Y. Cho, S. M. Lee, S. Chen, Z.-G. Zhang, Y. Li and C. Yang, *J. Mater. Chem. C*, 2019, **7**, 4716–4724.
38 W. Yang, Z. Luo, R. Sun, J. Guo, T. Wang, Y. Wu, W. Wang, J. Guo, Q. Wu, M. Shi, H. Li, C. Yang and J. Min, *Nat. Commun.*, 2020, **11**, 1218.
39 F. Eller, C. R. McNeill and E. M. Herzig, *Adv. Energy Mater.*, 2024, **14**, 2304455.
40 C. Liu, C. Xiao, C. Xie, Q. Zhu, Q. Chen, W. Ma and W. Li, *ChemPhysChem*, 2022, **23**, e202100725.
41 T. Wang, M.-S. Niu, Z.-C. Wen, Z.-N. Jiang, C.-C. Qin, X.-Y. Wang, H.-Y. Liu, X.-Y. Li, H. Yin, J.-Q. Liu and X.-T. Hao, *ACS Appl. Mater. Interfaces*, 2021, **13**, 11134–11143.
42 C. Wöpke, C. Göhler, M. Saladina, X. Du, L. Nian, C. Greve, C. Zhu, K. M. Yallum, Y. J. Hofstetter, D. Becker-Koch, N. Li, T. Heumüller, I. Milekhin, D. R. T. Zahn, C. J. Brabec, N. Banerji, Y. Vaynzof, E. M. Herzig, R. C. I. MacKenzie and C. Deibel, *Nat. Commun.*, 2022, **13**, 3786.
43 B. Ebenhoch, S. A. J. Thomson, K. Genevičius, G. Juška and I. D. W. Samuel, *Org. Electron.*, 2015, **22**, 62–68.
44 C. Liu, Z. Li, Z. Zhang, X. Zhang, L. Shen, W. Guo, L. Zhang, Y. Long and S. Ruan, *Phys. Chem. Chem. Phys.*, 2017, **19**, 245–250.
45 P. Schilinsky, C. Waldauf and C. J. Brabec, *Appl. Phys. Lett.*, 2002, **81**, 3885–3887.
46 M. Lenes, M. Morana, C. J. Brabec and P. W. M. Blom, *Adv. Funct. Mater.*, 2009, **19**, 1106–1111.
47 H. Feng, M. Li, W. Ni, B. Kan, Y. Wang, Y. Zhang, H. Zhang, X. Wan and Y. Chen, *Sci. China Chem.*, 2017, **60**, 552–560.
48 C. M. Proctor, C. Kim, D. Neher and T.-Q. Nguyen, *Adv. Funct. Mater.*, 2013, **23**, 3584–3594.